Non-Debye dielectric relaxation in biological structures arises from their fractal nature

Valerică Raicu,* Takayuki Sato, and Georgeta Raicu

Department of Physiology, Kochi Medical School, Nankoku 783-8505, Japan
(Received 3 January 2001; revised manuscript received 16 March 2001; published 27 July 2001)

What differentiates biological tissues from one another, thereby allowing their accomplishment of a physiological function, is their organization at supracellular and cellular levels. We developed general dielectric models for Cantorian (or treelike) fractal networks of transmission lines that mimic supracellular organization in numerous biological tissues and tissue surfaces, and which are compatible with both *in vitro* and *in vivo* measuring techniques. By varying a set of adjustable physical and geometrical parameters pertaining to the structure, we could numerically reproduce a variety of dielectric dispersion curves—most of them of a composite type—that suitably described experimental data from relatively organized biological tissues. We therefore conclude that the well-documented non-Debye dielectric behavior of biological structures reflects their self-similar architecture.

I. INTRODUCTION

Fractal organization of biological matter, viz, its construction in a repetitive or self-similar manner [1] is a fact of incontestable beauty and source of growing interest for the study of biological objects' architecture [2–4]. This design principle is thought to occur as a necessity for keeping to a minimum the amount of genetic information to be transmitted in the process of organism growing [1,3], for optimal functioning of the system with minimal consumption of energy [5], or for an increase in the surface/volume ratio in systems involving transport through surfaces [3], to cite but a few of the literature interpretations.

The method most widely used for investigating biological structures relies on textural analysis of sample sections, from which the observed features can be put in a quantitative form such as the fractal dimension [4]. Analysis of histological data [2,3,6] suggests that fractal structures in tissues fall into two main categories: (1) *percolating* or labyrinthine agglomerations of cells (e.g., liver parenchyma); and (2) *Cantorian* structures including branching vascular networks (in, e.g., lung, and plants leaves), and rough surfaces such as epithelia (e.g., skin) and cell membranes (in, e.g., lymphocyte and hepatocyte). The second category, which is of special interest in this work, owes its name to a mathematical concept known as the Cantor bar (or set) [1], which is obtained by repetitive division of a line segment into three or more segments and removing the middle ones (Fig. 1).

Unfortunately, however interesting and stimulating, morphological studies tell little, if at all, about how the structure determines the physical properties of a tissue as a whole to facilitate its accomplishment of a physiological function. By contrast, techniques based on transport phenomena in disordered systems [7] appear to answer this question, as transport phenomena are presumably affected by the type of structure involved and by the physical properties of its constituents [8–10]. Of these techniques, those based on transport of

electrical charge driven by alternating currents of variable frequencies, known generically as *impedance* [11] or *dielectric* [12] *spectroscopy*, are particularly useful, because of their added capability for *in vivo* investigations [13,14].

The interpretation of the results obtained from dielectric spectroscopy studies requires electrical models that relate the frequency spectra of permittivity and conductivity (alternatively, impedance modulus and phase) [15,16] to the electrical and structural characteristics of the tissue constituents (i.e., the cells). Classical dielectric theories for systems of cells rely on assumptions of high dilution and random distribution of cells within the sample and predict Debye-type frequency-dependent permittivity and conductivity both varying between low and high frequency plateaus [12,15,17]. Though such models have been successfully applied to dilute cell suspensions or to single cells [18], their underlying approximations no longer hold if the particles get closer to form more or less orderly aggregates. This may lead to an absence of the low frequency plateau from the dispersion curves, which has recently been well documented [10,19,20]. However, with rare exceptions [14], an electrodynamical treatment of particle aggregates is presently restricted to a two-particle system (see, for instance, Ref. [21]).

Fortunately, the fractal disposition of cells within most of biological tissues suggests a possible reformulation to the "aggregate" problem in terms of total impedance of fractal networks, which have been used earlier to model electrical properties of several systems including percolative structures [22], and rough metal-electrolyte interfaces [23–28]. Liu was the first to propose a deterministic resistor-capacitor (RC) network based on the Cantor bar model as a possible solution to the century-old problem of "anomalous" AC response of rough electrode/electrolyte interfaces [23]. Further refinements by Kaplan *et al.* [24,25] considered the effect of disorder as well as the possibility of interchanging the electrode and electrolyte to form the inverse Cantor bar model. Both Liu's original model and its subsequent modifications predicted that the impedance behaves at low frequencies as $(jf)^{-\eta}$ [which represents the constant-phase-angle (CPA) law with $j=(-1)^{1/2}$ and η being a function of the fractal dimension d of the interface]—a result that Sapoval *et al.*

————
*FAX: +81 88 8802310.
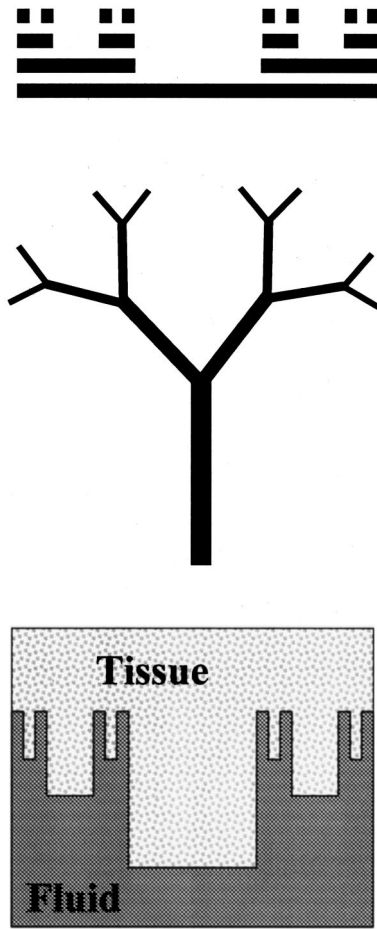Electronic address: vraicu@pop.med.kochi-ms.ac.jp

FIG. 1. Four-stage Cantor bar (top) and two Cantorian structures: fractal treelike vascular system (middle), and section of a tissue/fluid rough interface (bottom). The Cantor set is obtained by dividing a line segment into, for instance, three segments and removing the middle one, then repeating the operations for each remaining segment, and so on, until the desired level is reached.

[27] and Blunt [28] showed to be valid under limited conditions only. The way into the biological field has been opened for the Cantorian models by Sapoval [26], and later by Dissado and co-workers [8,29] who outlined the basic principles of applying fractal models in biodielectric studies. In spite of its remarkable potential of modeling biological structures [2–4], however, the fractal approach has been largely disregarded by biodielectricians, or, in the rare cases that it received attention, it was met by skepticism (see Ref. [15] for a typical opinion). This is because, while previous works on fractal structures have mostly sought to identify factors leading to the existence of the CPA law at low frequencies, no biological system has been identified whose dielectric properties show plain CPA behavior over a wide frequency range. In fact, biological tissues' dielectric response is usually more complex—sometimes composed of *two* (or more) elements of a CPA- or Debye-type, or combinations of them [10,20]. Grounded on a superficial reasoning, this may imply fractal models inadequacy.

To clarify whether the fractal approach still has a role to play in the interpretation of biodielectric data, we undertook a detailed study of branching deep-tissue structures and tissue surfaces by using a general Cantorian model based on the transmission line formalism in which, unlike most of the previous models, the line characteristics are distributed properties and are generally complex quantities. This facility is required since most parts of the real biological tissues are neither pure conductors nor pure dielectrics as considered in the case of metal/electrolyte interfaces. To allow for different branch geometries and/or intrinsic structures (such as the vessel walls in the case of vascular trees), the branch longitudinal and transverse electrical properties are let to scale independently, rather than being correlated as in the previous reports. Under these provisions, and upon proper choices of sets of electrical and geometrical parameters, we succeeded in stimulating a variety of composite dielectric dispersion spectra that are very similar to those obtained in experimental studies.

Details of our proposed model are given in Sec. II of this paper, for an electrode-tissue configuration compatible with *in vitro* investigations and for two additional configurations pertaining to *in vivo* studies of vascular trees and roughly surfaced epithelia. Models of the second type have not been proposed before; yet, most of the recent experimental studies on tissues are performed *in vivo* and would require consideration of pertinent models. In Sec. III, computer simulations of dispersion spectra are carried out for some particular cases thought of as illustrative for the dielectric behavior of biological structures. Comparative results for electrode configurations compatible with *in vitro* and *in vivo* situations are also presented. The dispersion spectra predicted by the present model are discussed in Sec. IV in connection with literature data and with the results we obtained from simulations with lumped-element (i.e., RC) Cantorian networks. In addition, some interesting findings regarding the uniqueness of the results of measurements on Cantorian fractals are discussed, and possible directions for future development are outlined. Section V concludes the paper summarizing the main results.

II. GENERAL ELECTRICAL MODEL FOR CANTORIAN FRACTALS

A. Problem formulation

Figure 2 schematizes a typical situation for impedance measurements of Cantorian-type fractal structures compatible with *in vitro* investigations (see later). For simplicity, we only illustrate the case for $N=2$ daughter branches emerging from parent branch at each branching point with all branches situated in the same plane, but the general admittance equations introduced in the next section hold for any N value and any spatial orientation of the branches. For identification of each branch, we use m as generation index within the tree, and n for individuals within their generation. For a system consisting of M generations of branches with $N \geq 2$, m varies from 0 to M-1, while n varies from 0 to N^n-1.

The equivalent circuit of the Cantorian structures in Fig. 2 (called hereinafter ''Model 1'') can be thought of as treelike network of transmission lines, in which parallel combinations of N branches of generation index $m+1$ provide termi-
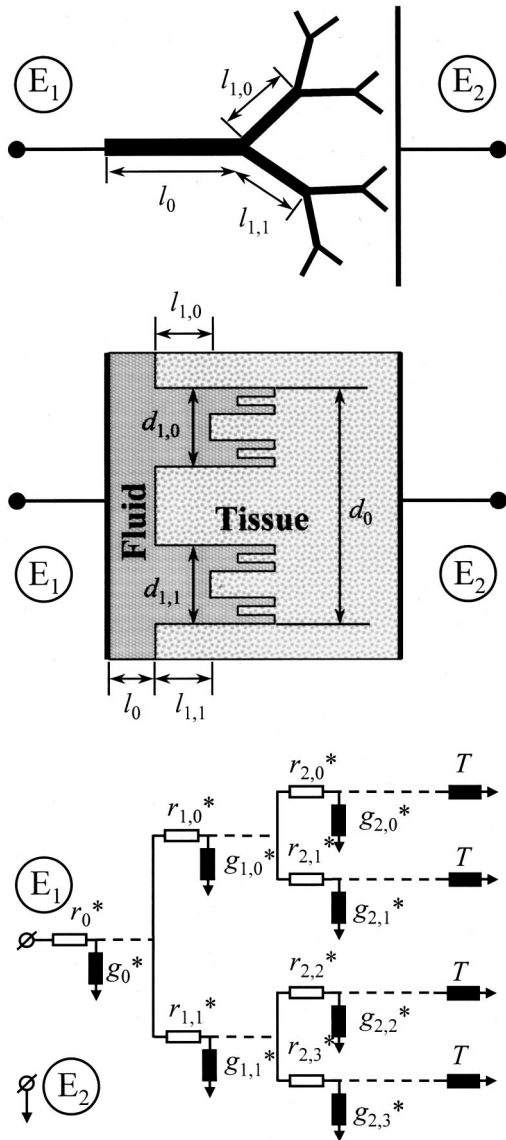
FIG. 2. Possible geometrical disposition of the measuring electrodes (E_1 and E_2) compatible with *in vitro* dielectric measurements (Model 1) on Cantorian deep-tissue structures (top) and interfaces (middle), and corresponding electrical circuit modeled as a fractal network of transmission lines (bottom). Geometrical characteristics of the first and second branch generations are also shown. Dashed lines signify that r^* and g^* are distributed parameters (i.e., R^* and G^* per unit length), while the asterisk indicates that they are complex quantities. Other symbols are described in the text.

nal admittances for each member of the mth generation. In this sense, electrical components $r_{m,n}^*$ and $g_{m,n}^*$ in the figure should be regarded as distributed parameters representing the longitudinal (complex) resistance per unit length of line (i.e., $R_{m,n}^*/L_{m,n}$), and the transverse (complex) conductance per unit length of line or the conductance between the lateral face of the line and the ground electrode (i.e., $G_{m,n}^*/L_{m,n}$). The termination admittance $T=G_T+j\omega C_T$ of the last generation of branches (index M-1) could be either a constant capacitance or conductance, or a more complicated frequency-dependent parameter, depending on the peculiari-

ties of the investigated system. For example, for rough surfaces, the underlying tissue provides termination admittances for the structure, while for a vascular tree in the lung, the terminal admittance represents the alveolar region including blood capillaries in the alveolar walls. If frequency dependent, the termination admittance will contribute additional subdispersions to the overall spectra, as also does any frequency dependence in the transverse conductance G^* or longitudinal resistance R^*. However, we will avoid such details in the present work, which intends to setup a framework for more detailed future analyses and reveal the main features of electrical phenomena occurring in dense biological systems.

As a general rule we shall comply within the calculations below, the letters m, n, and k are summation or multiplication indexes whenever they appear as subscripts of some symbols, and power exponents when appearing as superscripts. The same rule applies to the letter N with the specification that this also appears as an independent symbol standing for the branching degree, as defined above.

As one can readily see, the electrode configuration shown in Fig. 2 (Model 1), though easy to understand and intuitively appealing, can only be applied in *invasive* studies, which constitute a significant drawback from the biophysicist's point of view. More precisely, for a vascular tree, access of the E_1 electrode to the interior of the trunk can only be gained after sectioning the latter, a procedure that would affect the viability of the whole system. Similarly, for the roughly surfaced epithelia, placing one electrode under the skin would require skin excision. On the contrary, by placing the measuring electrodes on that side of the tissue that is naturally accessible to the investigator, as shown in Figs. 3 (Model 2) and 4 (Model 3), one would avoid the problem of invasiveness for both types of systems discussed, and would therefore be able to study the tissues *in vivo*. In these two cases, the equivalent circuits are modified as follows. For the vascular tree (Fig. 3), the two subtrees consisting of branches from generation 1 upward are serially connected, while for the rough interface (Fig. 4), the two subtrees are connected in parallel. (A very rigorous electrical modeling of the structure presented in Fig. 4 should consider also a serial coupling between the two (or more) substructures at the level of their termination admittances T.) In both cases, a complex stray conductance G_{ie}^* was added in parallel to the whole network to account for the current flow between electrodes through other pathways than the fractal network. This additional conductance has an experimental support, and has been previously investigated by us in connection with a superficial fluid layer intervening between the tissue surface and the tip of the measuring probe [19].

B. Input admittance of an individual branch modeled as a transmission line

According to the general theory of transmission lines [30], the input admittance measured at the downstream end of line m, n having the characteristic admittance $K_{m,n}$, propagation constant $\gamma_{m,n}$, and terminated by an admittance Y_t, due to N daughter branches (index $m+1$), may be expressed as
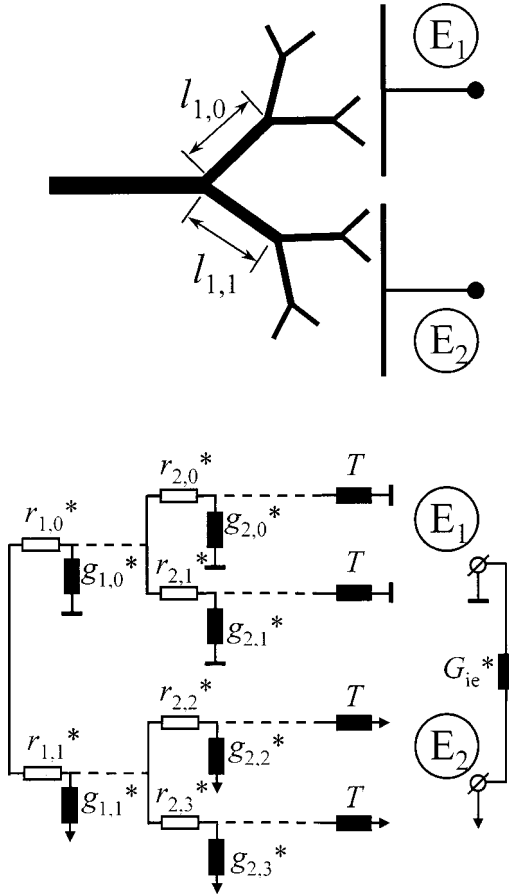
FIG. 3. Top: Possible geometrical disposition of the measuring electrodes (E_1 and E_2) compatible with *in vivo* dielectric measurements on Cantorian deep-tissue structures (Model 2). Bottom: Equivalent electrical circuit for the fractal network of transmission lines shown at the top. $G_{ie}^* = G_{ie} + j\omega C_{ie}$ is a stray conductance that directly connects the two electrodes (i.e., outside the fractal "route"). Other symbols, same as in Fig. 2.

$$Y_{m,n} = \frac{Y_t + K_{m,n}\tanh(\gamma_{m,n}L_{m,n})}{1 + (Y_t/K_{m,n})\tanh(\gamma_{m,n}L_{m,n})} \qquad (1)$$

with the transmission characteristics given by

$$K_{m,n}^2 \equiv g_{m,n}^*/r_{m,n}^* = G_{m,n}^*/R_{m,n}^*, \qquad (2)$$

$$\gamma_{m,n}^2 \equiv g_{m,n}^* r_{m,n}^* = G_{m,n}^* R_{m,n}^*/L_{m,n}^2. \qquad (3)$$

Next, assume that $G_{m,n}^*$ and $R_{m,n}^*$ change from one generation of branches to another by some factors to be defined below, due to changes in vessel size, position, and orientation with respect to the ground electrode. Because of self-similarity, if the properties of any single branch are known, then the properties of all other branches can be calculated recurrently. In particular, we shall relate the $G_{m,n}^*$ and $R_{m,n}^*$ of any branch m, n to those of the trunk of the tree, namely, $G_{0,0}^*$ and $R_{0,0}^*$ (or simply G_0^* and R_0^*). For this, we transiently employ the definitions $G_{m,n}^* = F_{m,n}L_{m,n}\sigma_t^*$ and $R_{m,n}^*$
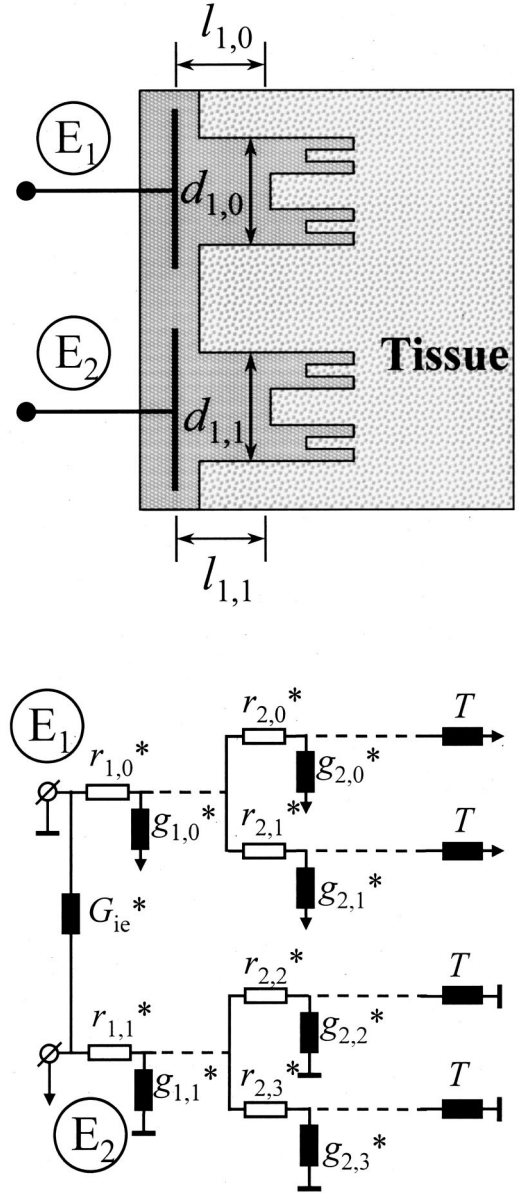
FIG. 4. Top: Possible geometrical disposition of the measuring electrodes compatible with *in vivo* dielectric measurements on Cantorian tissue/fluid interfaces (Model 3). Bottom: Equivalent electrical circuit for the fractal network of transmission lines shown at the top. $G_{ie}^* = G_{ie} + j\omega C_{ie}$, is a stray conductance that connects the two electrodes outside of the fractal "route." Other symbols, same as in Fig. 2.

$= (A_{m,n}\sigma_l^*)^{-1}L_{m,n}$, where σ_t^* is the transverse and σ_L^* is the longitudinal equivalent complex conductivity, $L_{m,n}$ and $A_{m,n}$ are the length and the transverse sectional area of the branch, while the factor $F_{m,n}$ depends on the branch dimensions other than $L_{m,n}$ and on its distance and orientation relative to the ground electrode. (If, for example, the branch is a cylinder of radius ρ_a coaxial with a cylindrical ground electrode of radius ρ_b, then $F = 2\pi/\ln(\rho_b/\rho_a)$.) Consequently, one can write down the following relations for transversal conductance and longitudinal resistance:

$$G_{m,n}^* = G_0^* \frac{F_{m,n}L_{m,n}}{F_{0,0}L_{0,0}}$$

$$= G_0^* \prod_{k=1}^{m} \frac{F_{k,[n/N^{m-k}]}L_{k,[n/N^{m-k}]}}{F_{k-1,[n/N^{m-k+1}]}L_{k-1,[n/N^{m-k+1}]}} \quad \text{for} \quad m \geq 1$$

$$= G_0^* \quad \text{for} \quad m,n = 0, \tag{4}$$

$$R_{m,n}^* = R_0^* \frac{A_{0,0}L_{m,n}}{A_{m,n}L_{0,0}}$$

$$= R_0^* \prod_{k=1}^{m} \frac{A_{k-1,[n/N^{m-k+1}]}L_{k,[n/N^{m-k}]}}{A_{k,[n/N^{m-k}]}L_{k-1,[n/N^{m-k+1}]}}, \quad \text{for} \quad m \geq 1$$

$$= R_0^* \quad \text{for} \quad m,n = 0, \tag{5}$$

where the symbol [ ] extracts the integer part of the number it contains.

The last forms of Eqs. (4) and (5) together with Eq. (1) provide means for computing the input admittance of any branch m, n, as we shall detail in the next section.

C. Total admittance of the fractal networks

To compute the total admittance of the structures presented in Fig. 2, as measured between E_1 and E_2, first consider the youngest generation of branches (index M-1) and compute their input admittances from Eq. (1) by ascribing values (see sections II A and III A 2) to the real and imaginary parts of terminal admittances T. Then, the total admittance of each group of N branches having the same mother branch provides terminal admittances, $Y_t = \sum_{k=0}^{N-1} Y_{m,nN+k}$, for the generation $m = M$-2; the process can be iterated down to the generation $m = 0$ (i.e., the trunk of the tree) until the input admittance of the whole structure is obtained ($Y_{\text{structure}} = Y_{0,0}$).

The admittance of the structures presented in Figs. 3 and 4 is computed by following the same procedure, except for the last step for which the iteration ends at generation 1. Then, the total admittance is computed by using the formulas for the series or parallel arrangements, depending upon the case.

It is to be mentioned that, in practice, the number of substructures lying beneath each electrode cannot, in general, be rigorously specified. In addition to this, the electrodes geometry may also affect the results of measurements. Our model thus describes the reality only on average. In fact this limitation is not purely theoretical; it has an experimental origin and reflects the difficulty to control the position relative to the electrodes of substructures within the tissue. The possible implications of such dependence of measurement results on the experimental conditions should not be disregarded, and we will turn our attention onto this matter later on in this work.

III. RESULTS

A. Approximations

To compute the total admittance of the structures discussed above, one needs to be more specific with regard to the choice of model parameters, which may depend upon the peculiarities of each tissue. However, we will not stick in this section to any particular tissue, as the main goal herein is to unveil the dielectric "signature" of Cantorian structures. For this, we will make some approximations to be described below.

1. Symmetrical tree

It is assumed that all branches in the same generation have the same size and that the diameter and length of branches only change by constant factors from one generation to another, which appears to be quite acceptable for the case of a vascular tree at least [2]. Consequently, the A, and l ratios in Eqs. (4) and (5) are constants independent of order m, n. In addition to this, F ratio is also considered constant, though the parameter F accounts for the position and orientation of the vessels with regard to the measuring electrodes, which might not be the same for all branches of the same generation. On these assumptions, we have

$$\frac{F_{k,[n/N^{m-k}]}L_{k,[n/N^{m-k}]}}{F_{k-1,[n/N^{m-k+1}]}L_{k-1,[n/N^{m-k+1}]}} \equiv a = \text{const},$$

$$\frac{A_{k-1,[n/N^{m-k+1}]}L_{k,[n/N^{m-k}]}}{A_{k,[n/N^{m-k}]}L_{k-1,[n/N^{m-k+1}]}} \equiv b = \text{const}$$

for any $1 \leq k \leq m$, and the multiple products in Eqs. (4) and (5) could be replaced by the simpler quantities a^m and b^m, so that

$$G_{m,n}^* = G_0^* a^m \tag{4'}$$

and

$$R_{m,n}^* = R_0^* b^m \tag{5'}$$

for any $0 \leq m \leq M-1$ and $0 \leq n \leq N^m - 1$.

2. Homogeneous branches

The intrinsic dielectric dispersions of the cells constituting the fractal structure are not considered, as they may only affect the shape of the dispersion curves at relatively high frequencies while our interest here is in elucidating the effect of tissue architecture. Accordingly, constant values were chosen for the real and imaginary parts of the electrical parameters R_0^*, G_0^*, and T. In particular, $G_0 = \text{Re}(G_0^*)$ was neglected to reflect the relatively low conductivity of the membranes of the cells bordering the structure (i.e., the branch wall), while $C_0 = \text{Im}(G_0^*)/\omega$ (with ω being the angular frequency) was varied as described below. Also, R_0^* was replaced by the quantity $L_0/(A_0 \sigma_L^*)$, where $\sigma_L^* = \sigma_L + j\omega\varepsilon_0\varepsilon_L$ with σ_L and ε_L the longitudinal electrical properties of the branch, and $\varepsilon_0 = 8.854 \times 10^{-12}$ F/m.

B. Computer simulations for the *in vitro* network model

The dispersion curves obtained from simulations with the network model compatible with in vitro measurements (Fig. 2) are shown in Figs. 5–7, for different sets of model param-
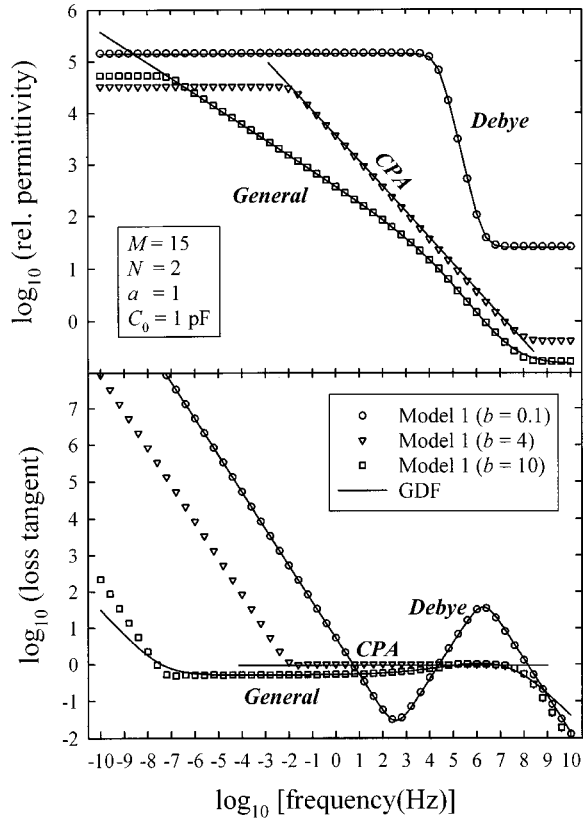
FIG. 5. Effect of variation of the geometrical parameter b defined in the text upon the simulated frequency spectra of relative permittivity and loss tangent of Model 1 (Fig. 2). R_0^*, computed (see text) from $\sigma_L = 0.6$ S/m, $\varepsilon_L = 70$, and $L_0/A_0 = 3.2 \times 10^4$ m^{-1}. T ($= G_T + j\omega C_T$), computed from $C_T = 1$ pF, and $G_T = 0$ S. Other parameters are shown in the inset. Also added (solid lines), simulations by the GDF [Eq. (6)] with parameters given in Table I.

eters that were considered as illustrative for the present work. The data (points) represented as relative dielectric constant and loss tangent vs frequency, were calculated by using a value of 9.4 mm for the measuring cell constant [13], which approaches the values for the probes employed in most of our previous studies of tissues (see, e.g., [19]).

As seen in Fig. 5, a family of dispersion curves with remarkable properties can be obtained upon variation of the model parameter b defined above. These curves were fitted to a general dispersion function (GDF) to be defined momentarily, and the best-fit parameters were collected in Table I together with the parameters corresponding to the subsequent figures. A special case of the GDF, which is relevant to the present work and which incorporates the Debye-type [31] functions and the "universal" response [32] as its particular cases, reads [10]:

$$\varepsilon^* \equiv \varepsilon - j\sigma/(2\pi f\varepsilon_0)$$

$$= \varepsilon_h + \frac{\Delta}{(jf/f_c)^\alpha + (jf/f_c)^{1-\beta}} + \frac{\sigma_l}{j2\pi f\varepsilon_0}, \qquad (6)$$

where the permittivity ε is relative to the value of free space ($\varepsilon_0 = 8.854 \times 10^{-12}$ F/m), σ is the conductivity, and l and h
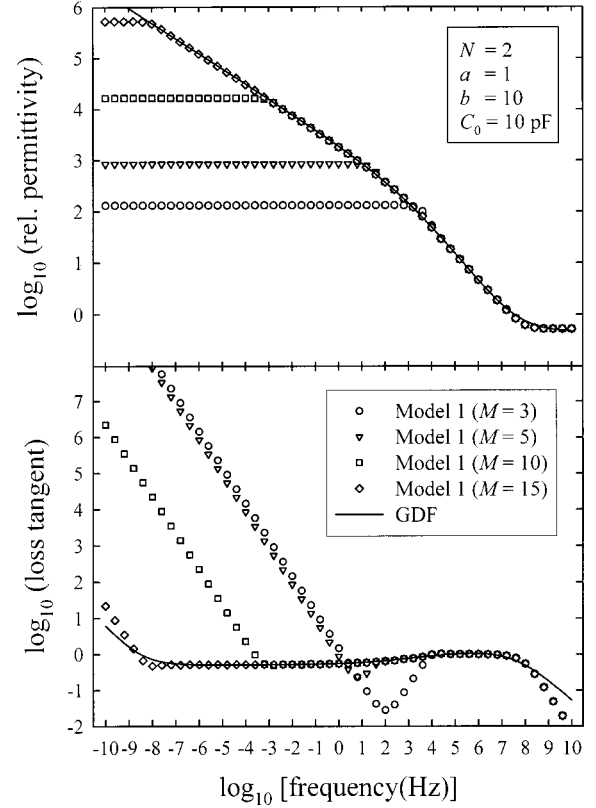
FIG. 6. Formation of the low frequency side of a nonclassical-type dispersion curve upon increasing the number of tree branches M of the structure shown in Fig. 2 (i.e., Model 1). Model parameters, as described in the legend to Fig. 5. Also added (solid lines), simulations by GDF [Eq. (6)] with the parameters given in Table I.

refer to the low and high frequencies f, respectively; α and β are real constants between 0 and 1; f_c is the characteristic frequency; and Δ is a dimensional constant. Aided by analysis with this function, the results presented in Fig. 5 reveal the following.

(i) For subunitary b values, dispersion curves of a pure Debye type [i.e., Eq. (6) with $\alpha = \beta = 0$] were generated, which are characterized by an abrupt decay of the permittivity between low and high frequency plateaus, and by a relatively narrow pick of the loss tangent.

(ii) Values of b significantly larger than unity bring about broadening of the permittivity curve, accompanied by a loss tangent curve flattening over a wide frequency range. As the lowest frequency available in biodielectric measurements hardly goes down to values of 1 mHz or so, due to technical limitations as well as to unavoidable experimental artifacts (such as electrode polarization), the plateau in the permittivity predicted by our simulations with the fractal model usually escapes experimental observation. This justifies our simplified representation of data by a descending straight line in Fig. 5 (i.e., Eq. 6 with $\alpha = 1 - \beta = 1/2$).

(iii) Further increase in b leads to important changes in the lower side of the dispersion spectra, so that the permittivity curve shows two CPA-type portions (i.e., straight lines of different slopes), to which two flat (constant) regions of the loss tangent are associated. Again, this non-Debye behav-
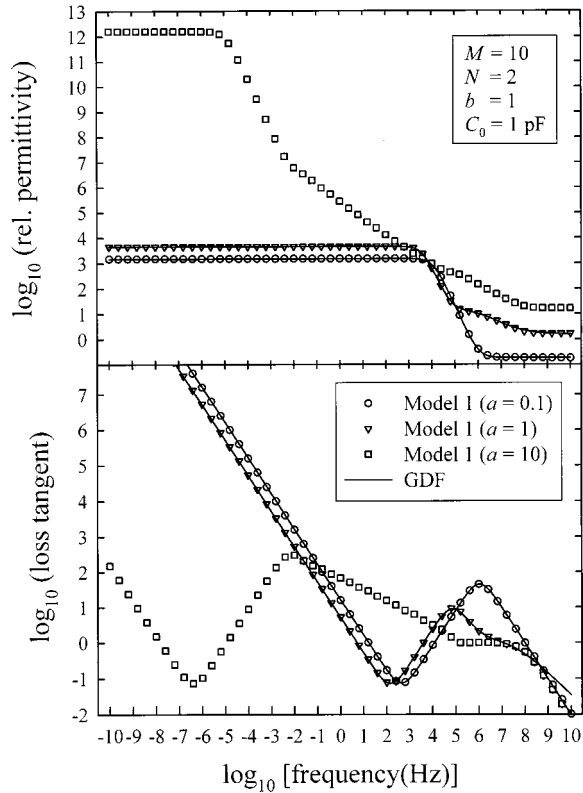
FIG. 7. Effect of variation of the geometrical parameter a upon the simulated frequency spectra of relative permittivity and loss tangent of the Cantorian structures in Fig. 2 (Model I). Model parameters, as described in the legend to Fig. 5. Also added (solid lines), simulations by GDF (Eq. 6) with the parameters listed in Table I.

ior of permittivity evolves into a low-frequency plateau that may not be experimentally detectable, and the general dispersion function [Eq. (6)] could be a good representation of the experimental data over a very wide frequency range, as illustrated in Fig. 5. As the asymptotic behavior of GDF [Eq. (6)] for $\alpha + \beta < 1$ is of the form $f^{-\alpha}$ for low frequencies and $f^{-(1-\beta)}$ for high frequencies, the two CPA characteristics have slopes $-\alpha$ and $-(1-\beta)$. This type of response may be regarded as a generalization of Jonscher's universal response [32,33].

To further illustrate the way a general dispersion spectrum arises from the fractal model, the results of simulations for different values of the number of branch generations M are

plotted in Fig. 6. It is seen how the low-frequency CPA component is progressively built upon addition of responses from different generations of branches. From the comparison between Figs. 5 and 6 for $b = 10$, one can also infer that variation of C_0 leaves the parameter α in Eq. (6) unchanged (i.e., it preserves the type of response), while modifying the values of the other parameters (see Table I).

Keeping the parameter b constant and varying the parameter a, which defines the ratio between the longitudinal resistance of successive tree branches, one obtains dispersion curves of a composite type, in fact, combinations of the known types of dispersion, as shown in Fig. 7 (see also the corresponding rows of Table I). Thus, by increasing the parameter a, the single Debye dispersion transforms into a combination of a Debye-type term at low frequencies and a Cole-Cole type one at high frequencies. Larger a values introduce a component of an unclassified type between the two Debye-type dispersions, which has itself a composite nature. For this latter case, a proper fit by one or two GDF terms was, evidently, not possible.

Variation of other model parameters could be also studied (as we actually did), but this reveals dispersion curves of the same types as those already discussed.

C. Simulations for the *in vivo* network models

As mentioned above, in the practice of dielectric measurements on biological tissues, *in vivo* techniques are generally preferred to the *in vitro* ones. It was therefore of interest for this study to find out the differences that may occur between the results of *in vivo* (Figs. 3 and 4) and *in vitro* (Fig. 2) measurements of the same Cantorian structure.

The comparative results for all three models presented in this paper are shown in Fig. 8. As seen, the parallel-type combination of the two subtrees (Model 3) gives a much higher permittivity than both the *in vitro* (Model 1) and the *in vivo*-series (Model 2) configurations throughout the investigated frequency range, while differences between the ε values for Models 1 and 2 occurred at high frequencies only, as reflected by different values of the ε_h in Table II. On the other hand, the low frequency sides of the loss tangent spectra of both *in vivo* cases differed markedly from those obtained for the Model 1, owing to very different values taken by the σ_i parameter (see Table II). Furthermore, almost no difference was found between the Model 2 and Model 1 for $G_{ie}^* = 0 + 0j$, while Model 3 gave still distinct results in this case, as reflected by the parameters presented in Table II.

TABLE I. Parameters corresponding to the best-fit simulations by Eq. (6) (lines) of the data (points) in Figs. 5–7.

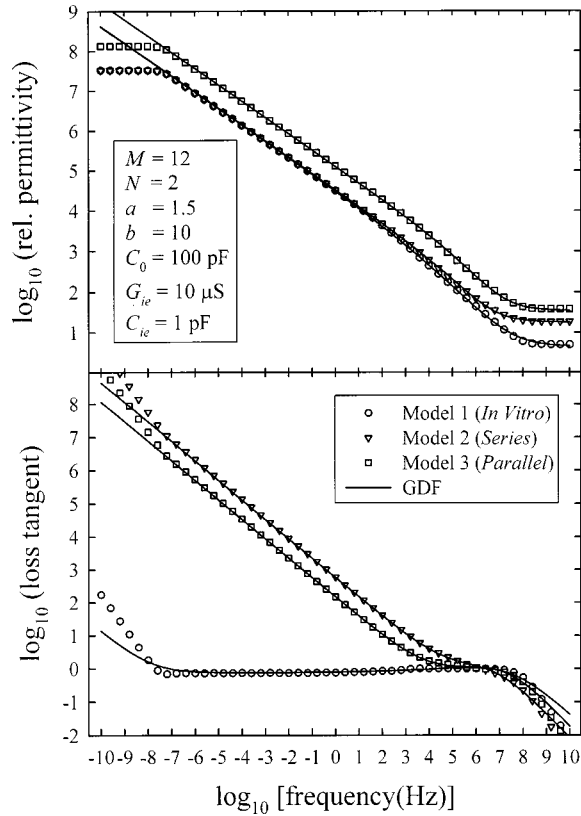| Fig. No.	Dispersion type	α_1	β_1	Δ_1	f_{c1} (Hz)	α_2	β_2	Δ_2	f_{c2} (Hz)	ε_h	σ_l (S/m)
5	Debye	0.00	0.00	1.4×10^5	2.5×10^4					25	4.1×10^{-5}
5	CPA (Universal)	0.50	0.50	1	1.0×10^8					0.35	1.5×10^{-8}
5	General	0.30	0.36	15	7.0×10^4					0.15	6.5×10^{-14}
6	General	0.30	0.38	2.0×10^2	3.7×10^3					0.46	6.0×10^{-14}
7	Debye	0.00	0.00	1.5×10^3	1.2×10^4					0.18	1.4×10^{-6}
7	Debye+Cole-Cole	0.00	0.00	4.5×10^3	4.0×10^3	0.00	0.38	13.9	1.8×10^6	1.55	1.3×10^{-6}

FIG. 8. Dispersion spectra of a Cantorian structure *in vitro* (Fig. 2—Model 1) as compared to those predicted by the *in vivo* models presented in Figs. 3 (Model 2) and 4 (Model 3). Also added (solid lines), simulations by GDF [Eq. (6)] with the parameters given in Table II. C_{ie} and G_{ie} apply to Models 2 and 3 only. Other parameters: R_0^*, computed (see text) from $\sigma_L = 0.6$ S/m, $\varepsilon_L = 70$, and $L_0/A_0 = 7.96 \times 10^3$ m^{-1}; T ($= G_T + j\omega C_T$), computed from $C_T = 1$ pF, and $G_T = 0$ S.

(For simplicity, data corresponding to $G_{ie}^* = 0 + 0j$ were not plotted in Fig. 8).

The near identity between the permittivity curves of the *in vivo* series and the *in vitro* models seen in Fig. 8 at frequencies lower than ~ 10 kHz may appear paradoxical when judging based on a lumped-circuit-elements model. However, the paradox is only apparent, as the effect is due to the distributed parameters formalism used in the present work and to the particular circumstance that the branch wall conductivity G_0 has been neglected in our numerical simulations. Evidently, this last approximation does not necessarily

hold true for biological tissues over an indefinite frequency range, but it appears rather good at subradio frequencies, to which our above discussion refers.

IV. DISCUSSION

A. Comparison with the literature data

The "general" type of dispersion presented in Figs. 5 and 6 exhibits striking similarities with the data from measurements on the human skin (see Fig. 2 of Ref. [20]) over a wide frequency range, which could be remarkably well fitted to Eq. (6), both for wet (with physiological saline) and dry (i.e., untreated) skin surface. To be meticulous, however, there are indications in the above-cited data that two terms of the general type [Eq. (6)] would be even more suitable. This is what would have been actually expected for the skin having both a rough surface and a network of capillaries (possibly of a fractal type) lying underneath, which, according to the present model, could well lead to a two-terms dispersion.

Nearly the same type of dispersion as above has been obtained experimentally for the lung tissue (see, e.g., [34]). Thus, our model may furnish the necessary link between the well-documented fractal (treelike) structure of the airways and the blood vessels in the lung [3,35], and its non-Debye dielectric characteristics, although combined dielectric-morphometric experimental studies would be required for a well-grounded conclusion in this respect.

Less expectedly within the framework of this paper, characteristics of the "general" type have been obtained from measurements on liver [10,19] as well as on other biological tissues [36] whose structure belongs to the class of percolation fractals mentioned in the introduction section. However, the two types of structures may present profound similarities at the level of the general laws of transport phenomena on fractal lattices [37], which may explain our findings.

It should be also mentioned that simple Debye-type dispersion curves as shown in Fig. 5 have not been observed in biological tissues. This is probably because morphometric data do not support subunitary b values (in e.g., rat lung, an average b value ~ 1.7 can be calculated from morphological data [38]).

B. Distributed vs lumped circuit parameters

As stated in the Introduction, literature models for Cantorian systems [23–28] made no allotment for independent scaling of the transversal and longitudinal branch electrical

TABLE II. Parameters corresponding to the best-fit simulations by Eq. (6) (lines) of the data (points) in Fig. 8.

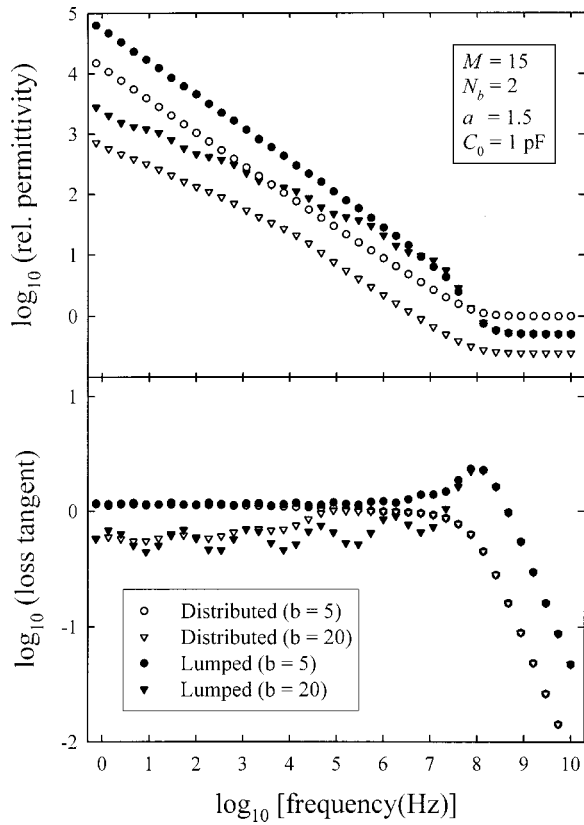| Model	α	β	Δ	f_c (Hz)	ε_h	σ_l (S/m)
1	0.41	0.36	310	1.5×10^5	5	3.0×10^{-11}
$2(G_{ie}^* \neq 0)$	0.41	0.26	130	1.3×10^6	18	1.1×10^{-3}
$2(G_{ie}^* = 0 + 0_j)$	0.41	0.30	140	1.2×10^6	6	2.8×10^{-11}
$3(G_{ie}^* \neq 0)$	0.41	0.26	420	2.0×10^6	35	1.1×10^{-3}
$3(G_{ie}^* = 0 + 0j)$	0.41	0.29	430	1.9×10^6	24	1.2×10^{-10}

FIG. 9. Comparison between the dispersion spectra simulated from the fractal distribution of transmission lines in Fig. 2 (Model 1) and from its corresponding lumped (RO) elements network. Parameters not shown in the inset were the same as in the legend to Fig. 8.

characteristics (reflected in our models by the independent parameters a and b), and/or neglected the capacitive component along the tree branches—a parameter that is however experimentally required, as it ensures finiteness of the limiting permittivity at high frequencies ε_h. The advantage of including two independent scaling parameters a and b presented by our models is apparent from analysis of the data in the results section, while possible implications for biodielectric studies were briefly discussed in the preceeding section. There only remains here the identification of those features distinguishing the dispersion spectra of a distribution of coaxial lines from those of the RC network models. One of the previous studies [25] has also considered the Cantorian distribution of transmission lines, but in addition to presenting some of the above-mentioned limitations that study was focused on the low frequency limit of the impedance.

In Fig. 9 we have plotted the frequency characteristics for two sets of model parameters corresponding to the *in vitro* model (Model 1) presented in Fig. 2 and its RC version. As seen, Model 1 predicts ε curves with one or two CPA components, depending on the chosen parameters, while the RC network predicts a component of a more or less CPA type followed by a rapid, quasi-Debye, drop in ε at very high frequencies, accompanied by a peak in the loss tangent. It is seen that, for relatively large b values, the curves obtained from the RC model simulations are significantly more

"wavy" than those predicted by Model 1. This seriously restricts the applicability of RC network models, since experimental curves are usually smoother.

C. Possible multiplicity of the results

Determination of permittivity ε and conductivity σ of biological tissues is usually based on an assumption that simple proportionality relations connect the two quantities to the measured C and G, namely, $C = k_{cell}\varepsilon$ and $G = k_{cell}\sigma$, where k_{cell} is the cell constant. Dielectric spectroscopists' preference for use of ε and σ over the Z (or Y) modulus and phase is generally justified by the independence of ε and σ on the sample (and probe) geometry and size. This reminiscence from dielectric studies of biological cell suspensions tacitly assumes that the sample is isotropic on large scales, which means that system's constituting elements (i.e., the cells) are distributed at random, which is generally not so for biological tissues. Thus, the use of k_{cell} value determined from measurements on homogeneous saline solutions is no longer acceptable, since the true cell constant can be different for different tissue structures. Unfortunately however, the cell constant of a given configuration of electrodes placed on a particular tissue cannot be *a priory* known, since it requires the knowledge of tissue equivalent electrical properties. The latter in turn requires the knowledge of the former, and this generates a circular reasoning.

According to the above discussion, neither the impedance, nor the permittivity would make any easier the representation of data from strongly heterogeneous (on large scales) biological systems such as the skin and the lung, and one should expect a multiplicity of results in measurements, depending on the particular geometry of the measuring cell and on its position relative to the tissue sample. This is, in fact, in agreement with our own experience with dielectric measurements on biological tissues, and may have profound implications for understanding the process of measurement of physical properties of biological systems, with special regard to the uniqueness of the results. It therefore appears that any communication of the results obtained from dielectric measurements on tissues should not only include information on the type of probe used and its cell constant but also on probe dimensions as well as its position relative to the tissue sample.

D. Model limitations

The present study is by no means definitive, and further developments of the model could take into account; the tree asymmetry, which implies that one branch divides into branches of different order [38,39], and the contribution of cells to the vascular wall electrical characteristics and to the terminal admittances. In fact, the equivalent complex conductance of the vascular wall can be readily incorporated into the present model, provided that the precise composition of the wall is known. Our preliminary investigations along these lines, however, revealed that the basic findings of the present report—viz., the nonclassical character of the dielectric response of fractal structures—are not essentially altered by such refinements in the theory.

V. CONCLUSION

We have presented a general electrical model for Cantorian structures with application to rough surfaces and vascular trees in biological systems. In addition to providing a variety of dispersion curves, our model could mimic most of the dispersion curves obtained from tissues with corresponding Cantorian structures, which generally have neither a Debye-type, nor a simple CPA-type behavior. We believe that these observations may open the door to a realistic approach to the longstanding problem of modeling transport phenomena in biological structures.

[1] B. B. Mandelbrot, *The Fractal Geometry of Nature* (Freeman, San Francisco, 1982).

[2] D. L. Turcotte, J. D. Pelletier, and W. I. Newman, J. Theor. Biol. **193**, 577 (1998).

[3] E. R. Weibel, Am. J. Phys. **261**, L361 (1991).

[4] J. E. McNamee, J. Appl. Physiol. **71**, 1 (1991).

[5] G. B. West, J. H. Brown, and B. J. Enquist, Science **276**, 122 (1997); A. I. Popescu, Acta Biotheor. **46**, 299 (1998).

[6] D. W. Fawcett, *Bloom and Fawcett: A Textbook of Histology* (Chapman and Hall, New York, 1996).

[7] M. Köpf, C. Corinth, O. Haferkamp, and T. F. Nonnenmacher, Biophys. J. **70**, 2950 (1996); G. A. Niklasson, J. Appl. Phys. **62**, R1 (1987).

[8] L. A. Dissado, Phys. Med. Biol. **35**, 1487 (1990).

[9] Y. Feldman, N. Kozlovich, Y. Alexandrov, R. Nigmatullin, and Y. Ryabov, Phys. Rev. E **54**, 5420 (1996); Y. Gefen, A. Aharony, and S. Alexander, Phys. Rev. Lett. **50**, 77 (1983); Y. Gefen, A. Aharony, B. B. Mandelbrot, and S. Kirkpatrick, *ibid.* **47**, 1771 (1981); Y. Gefen, B. B. Mandelbrot, and A. Aharony, *ibid.* **45**, 855 (1980).

[10] V. Raicu, Phys. Rev. E **60**, 4677 (1999).

[11] A. H. Kyle, C. T. Chan, and A. I. Minchinton, Biophys. J. **76**, 2640 (1999).

[12] K. Asami, in *Handbook on Ultrasonic and Dielectric Characterization: Techniques for Suspended Particulates*, edited by V. A. Hackley and J. Texter (The American Ceramic Society, Westerville, 1998), p. 333.

[13] V. Raicu, Meas. Sci. Technol. **6**, 410 (1995).

[14] V. Raicu, T. Saibara, H. Enzan, and A. Irimajiri, Bioelectrochem. Bioenerg. **47**, 333 (1998).

[15] K. R. Foster and H. P. Schwan, in *Handbook of Biological Effects of Electromagnetic Fields*, edited by C. Polk and E. Postow (CRC, Boca Raton, 1996), p. 25.

[16] M. E. Valentinuzzi, Crit. Rev. Biomed. Eng. **24**, 223 (1996).

[17] H. Pauly and H. P. Schwan, Z. Naturforsch. B **14**, 125 (1959); A. Irimajiri, T. Hanai, and A. Inouye, J. Theor. Biol. **78**, 251 (1979).

[18] S. Archer, H. Morgan, and F. J. Rixon, Biophys. J. **76**, 2833 (1999); J. Yang, Y. Huang, X. Wang, X. B. Wang, and F. F. Becker, *et al.*, *ibid.* **76**, 3307 (1999); V. Raicu, G. Raicu, and G. Turcu, Biochim. Biophys. Acta **1274**, 143 (1996).

[19] V. Raicu, T. Saibara, and A. Irimajiri, Bioelectrochem. Bioenerg. **47**, 325 (1998).

[20] V. Raicu, N. Kitagawa, and A. Irimajiri, Phys. Med. Biol. **45**, L1 (2000).

[21] A. V. Radchik, A. V. Paley, G. B. Smith, and A. V. Vagov, J. Appl. Phys. **76**, 4827 (1994).

[22] J. P. Clerc, G. Giraud, J. M. Laugier, and J. M. Luck, J. Phys. A **18**, 2565 (1985); L. A. Dissado and R. M. Hill, Phys. Rev. B **37**, 3434 (1988); S. Kirkpatrick, in *III-Condensed Matter*, Proceedings of Les Houches Summer School, edited by R. Balian, R. Maynard, and G. Toulouse (North-Holland, Amsterdam, 1979), Vol. 31, p. 321.

[23] S. H. Liu, Phys. Rev. Lett. **55**, 529 (1985); S. H. Liu, Solid State Phys. **39**, 207 (1986).

[24] T. Kaplan and L. J. Gray, Phys. Rev. B **32**, 7360 (1985); T. Kaplan, L. J. Gray, and S. H. Liu, *ibid.* **35**, 5379 (1987).

[25] T. Kaplan, S. H. Liu, and L. J. Gray, Phys. Rev. B **34**, 4870 (1986).

[26] B. Sapoval, Acta Stereol. **6**, 785 (1987).

[27] B. Sapoval, J.-N. Chazalviel, and Peyriere, Phys. Rev. A **38**, 5867 (1988).

[28] M. Blunt, J. Phys. A **22**, 1179 (1989).

[29] L. A. Dissado, J. M. Alison, R. M. Hill, D. A. McRac, and M. A. Esrick, Phys. Med. Biol. **40**, 1067 (1995).

[30] N. Marcuvitz, *Waveguide Handbook* (Dover Publications, New York, 1951); H. P. Schwan, in *Physical Techniques in Biological Research*, edited by W. L. Nastuk (Academic, New York, 1963).

[31] P. Debye, *Polar Molecules* (The Chemical Catalog Company, New York, 1929); K. S. Cole and R. H. Cole, J. Chem. Phys. **9**, 341 (1942).

[32] A. K. Jonscher, *Universal Relaxation Law* (Chelsea Dielectrics, London, 1996).

[33] A. K. Jonscher, Nature (London) **267**, 673 (1977).

[34] A. J. Surowiec, S. S. Stuchly, M. Keaney, and A. Swarup, IEEE Trans. Biomed. Eng. **34**, 62 (1987); S. Gabriel, R. W. Lau, and C. Gabriel, Phys. Med. Biol. **41**, 2271 (1996).

[35] M. F. Shlesinger and B. J. West, Phys. Rev. Lett. **67**, 2106 (1991).

[36] S. Gabriel, R. W. Lau, and C. Gabriel, Phys. Med. Biol. **41**, 2251 (1996).

[37] B. A. Huberman and M. Kerszberg, J. Phys. A **18**, L331 (1985).

[38] Z. L. Jiang, G. S. Kassab, and Y. C. Fung, J. Appl. Physiol. **76**, 882 (1994).

[39] W. Huang, R. T. Yen, M. McLaurine, and G. Bledsoe, J. Appl. Physiol. **81**, 2123 (1996).